Direct Versus Indirect Line of Sight (LOS) Stabilization

Peter J. Kennedy, *Member, IEEE,* and Rhonda L. Kennedy, *Member, IEEE*

***Abstract*—Two methods are analyzed for inertially stabilizing the pointing vector defining the line of sight (LOS) of a two-axis gimbaled laser tracker. Mounting the angular rate and acceleration sensors directly on the LOS axes is often used for precision pointing applications. This configuration impacts gimbal size, and the sensors must be capable of withstanding high angular slew rates. With the other stabilization method, sensors are mounted on the gimbal base, which alleviates some issues with the direct approach but may be less efficient, since disturbances are not measured in the LOS coordinate frame. This paper investigates the impact of LOS disturbances and sensor noise on the performance of each stabilization control loop configuration. It provides a detailed analysis of the mechanisms by which disturbances are coupled to the LOS track vector for each approach, and describes the advantages and disadvantages of each. It concludes with a performance comparison based upon simulated sensor noise and three sets of platform disturbance inputs ranging from mild to harsh disturbance environments.**

***Index Terms*—Angular rate sensor, gimbal, rate gyro, stabilization.**

I. Introduction

THE REQUIREMENT to point a laser from a dynamic platform continues to surface in both defense and communication applications. The laser and track sensor (i.e., camera, detector array, etc.) are mounted on the inner axis of a multiaxis mechanical gimbal; or below the gimbal, coupled to the line of sight (LOS) via a stabilized pointing mirror. Pointing control is implemented via two servo loops, the outer track or pointing loop and an inner stabilization or rate loop. The track sensor detects the laser returns from the target location. The track processor uses this information to generate rate commands that direct the gimbal bore-sight toward the target LOS. The stabilization loop isolates the laser and sensor from platform motion and disturbances that would otherwise perturb the aim-point. The track loop must have sufficient bandwidth to track the LOS kinematics. The stabilization loop bandwidth must be high enough to reject the platform disturbance spectrum. A typical configuration is illustrated in Fig. 1.

Disturbances that affect the pointing vector arise from platform angular motion or maneuvers, and external loads such as wind and air-stream induced torque. Platform linear motion and vibration generate disturbance torques due to mass imbalance and gimbal geometry. Conventional stabilization techniques employ rate gyros, rate integrating gyros, or rate sensors to sense rate disturbances about the LOS. They are often mounted on the inner gimbal axis, as close as possible to the gimbal bore-sight (i.e., I_x in Fig. 1), or in some application at the gimbal base. The mounting configuration can have a significant impact on pointing performance.

This paper focuses on two methods of implementing the stabilization servo loop design. A two-axis gimbal (El over Az), as shown in Fig. 1, is considered. Direct LOS stabilization, with the angular rate sensors mounted on the LOS axes, is normally recommended for precision pointing applications [1], [2]. The technique is simple to implement, requiring only two rate sensors and the associated rate loop compensation. Gimbal size is impacted, since a larger payload volume is required to mount the sensors on the inner gimbal. For high-performance aircraft applications, the penalty in drag and turbulence induced by a large gimbal penetrating the air-stream may be severe. In addition, the sensors must be capable of functioning, or at least withstanding, high angular rates generated during slew.

With indirect LOS stabilization, currently being pursued for several applications, the rate sensors are mounted on the gimbal base. This can alleviate some of the problems associated with the direct stabilization approach. The disturbances, however, are not measured in the LOS coordinate frame, which can degrade performance. The base mounted sensors must accurately measure the rates at the gimbal base. A processor transforms them to an equivalent disturbance about the LOS. A rate loop feedforward compensator applies a control signal proportional to the estimated rates, attempting to cancel the disturbances. The relationship between the actual LOS disturbances and those measured at the base of the gimbal is dependent upon gimbal geometry, structural rigidity, resolver accuracy, tachometer and/or encoder accuracy, and the processor sampling rate (if the control signal is processor generated). This method is more complex than the direct approach.

II. Gimbal Kinematic Relationships

Three coordinate frames are used to define gimbal motion, starting with the gimbal base frame (B), followed by the gimbal outer frame (O), and finally the gimbal inner frame (I). LOS elevation control is exercised via the inner gimbal y-axis, while azimuth control is applied via the outer gimbal z-axis. It is important to note that stabilization is required about the inner gimbal z-axis, called cross elevation. Therefore, the cross-elevation axis is actually controlled indirectly. The coordinate trans-

Manuscript received November 30, 2000; revised March 15, 2002. Manuscript received in final form October 1, 2002. Recommended by Associate Editor D. W. Repperger.

The authors are with David H. Pollock Consultants, Inc., Sensor Technology Specialists, Westwood, NJ 07675 USA (e-mail: dpollock@dhpconsultants.com).

Digital Object Identifier 10.1109/TCST.2002.806443

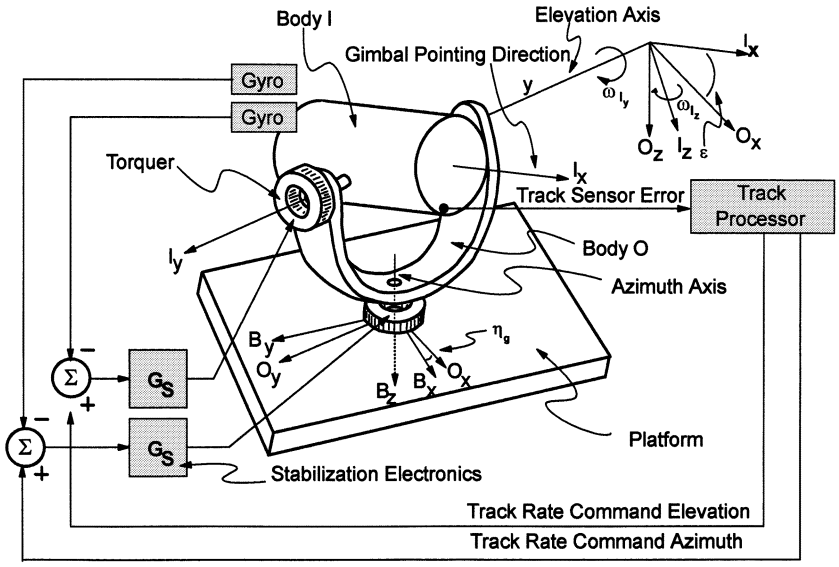

Fig. 1. Two-axis tracker configuration.

formation between the base and outer coordinate frame is (note a "bar" denotes a matrix, and a "hat" denotes a vector)

$$\overline{R}_\eta = \begin{bmatrix} c_\eta & s_\eta & 0 \\ -s_\eta & c_\eta & 0 \\ 0 & 0 & 1 \end{bmatrix}; \quad c_\eta = \cos(\eta); \quad s_\eta = \sin(\eta)$$

$\eta(t)$—relative azimuth angle between the outer and base coordinate frames.

The base coordinate frame rate vector $\hat{\omega}_B(t)$ is related to the outer coordinate frame rate vector $\hat{\omega}_O(t)$ by

$$\hat{\omega}_O(t) = \overline{R}_\eta(t)\hat{\omega}_B(t) + \hat{\dot{\eta}}(t) \tag{1}$$

where

$$\hat{\dot{\eta}}(t)^T = [0 \quad 0 \quad \dot{n}(t)]$$
$$\dot{\eta}(t) = \omega_{Oz}(t) - \omega_{Bz}(t).$$

The coordinate transformation between the outer and inner gimbal coordinate frame is given by

$$\overline{R}_\varepsilon(t) = \begin{bmatrix} c_\varepsilon & 0 & -s_\varepsilon \\ 0 & 1 & 0 \\ s_\varepsilon & 0 & c_\varepsilon \end{bmatrix}; \quad c_\varepsilon = \cos(\varepsilon); \quad s_\varepsilon = \sin(\varepsilon)$$

$\varepsilon(t)$—relative elevation angle between inner and outer gimbal coordinate frames.

The outer coordinate frame rate vector is related to the inner coordinate frame rate vector, $\hat{\omega}_I(t)$, by

$$\hat{\omega}_I(t) = \overline{R}_\varepsilon(t)\hat{\omega}_O(t) + \hat{\dot{\varepsilon}}(t) \tag{2}$$

$$\hat{\dot{\varepsilon}}(t)^T = [0 \quad \dot{\varepsilon}(t) \quad 0]; \qquad \dot{\varepsilon}(t) = \omega_{Iy}(t) - \omega_{Oy}(t).$$

The relationship between the angular acceleration of the inner and outer gimbal coordinate frames is obtained by differentiating (2) or

$$\hat{\dot{\omega}}_I(t) = \overline{R}_\varepsilon(t)\hat{\dot{\omega}}_O(t) + \overline{Q}_\varepsilon(t)\hat{\omega}_O(t)\dot{\varepsilon}(t) + \hat{\ddot{\varepsilon}}(t) \tag{3}$$

where

$$\overline{Q}_\varepsilon(t) = \begin{bmatrix} -s_\varepsilon & 0 & -c_\varepsilon \\ 0 & 0 & 0 \\ c_\varepsilon & 0 & -s_\varepsilon \end{bmatrix}.$$

III. Gimbal Dynamics Model

The gimbal dynamics model can be derived from the torque relationships about the inner and outer gimbal body axes based on rigid body dynamics. The expression for the inner gimbal angular dynamics is given by ("$\times$" denotes the cross product operation)

$$\overline{J}_I\hat{\dot{\omega}}_I(t) + \left(\hat{\omega}_I(t) \times \overline{J}_I\hat{\omega}_I(t)\right) = \hat{L}_I(t). \tag{4}$$

where sum of the kinematic torques about the inner gimbal, $\hat{L}_I(t)$, is

$$\hat{L}_I(t) = \begin{bmatrix} T_{Ix}(t) \\ T_{el}(t) \\ T_{Iz}(t) \end{bmatrix} - \begin{bmatrix} T_{Ulx}(t) \\ T_{Uly}(t) \\ T_{Ulz}(t) \end{bmatrix} - \begin{bmatrix} 0 \\ T_{If\omega}(t) \\ 0 \end{bmatrix}$$

with

$T_{If\omega}(t)$	Friction and cable restraint torques.
$\overline{J}_I$	Inner gimbal inertia matrix.
$T_{Ix}(t)$, $T_{Iz}(t)$	Reaction torques exerted by inner gimbal on outer gimbal.
$T_{UIx}(t)$, $T_{Uly}(t)$, $T_{UIz}(t)$	Mass imbalance torques about each gimbal axis.
$T_{el}(t)$	Elevation stabilization control torque.

The friction and cable restraint torques generate both linear and nonlinear disturbances, [3]. To simplify the analysis, it is assumed that the gimbal rotation axes are aligned with the principal axes of inertia so that the inertia matrix is diagonal and the inner gimbal dynamics equation can then be expanded as

$$T_{Ix} = J_{Ix}\dot{\omega}_{Ix} + \omega_{Iy}\omega_{Iz}(J_{Iz} - J_{Iy}) + T_{Ulx} \tag{5}$$

$$J_{Iy}\dot{\omega}_{Iy} = -\omega_{Iz}\omega_{Ix}(J_{Ix} - J_{Iz}) + T_{el} - T_{Uly} - K_{If}\dot{\varepsilon} - K_{I\omega}\varepsilon - T_{I,\,\mathrm{fric}} - T_{I,\,CR} \tag{6}$$

$$T_{Iz} = J_{Iz}\dot{\omega}_{Iz} + \omega_{Ix}\omega_{Iy}(J_{Iy} - J_{Iz}) + T_{UIz} \tag{7}$$

where

K_{If}	viscous friction coefficient;
$K_{I\omega}$	cable restraint coefficient;
T_{el}	$= T_{I\mathrm{rate}} + T_{I\mathrm{base}}$; $T_{If\omega} = T_{I,\,\mathrm{fric}} + T_{I,\,CR} + K_{If}\dot{\varepsilon} + K_{I\omega}\omega$;
$T_{I,\,\mathrm{fric}}$	nonlinear friction torques;
$T_{I,\,CR}$	nonlinear cable restraint torques.

In (5)–(7), and those equations that follow, the explicit dependency on time, (t), has been suppressed in the expanded expressions where no confusion will arise. The reaction torques on the outer gimbal are determined from (5) and (7). The elevation control axis is the inner gimbal y-axis, whose dynamics are generated by (6). The inputs to this equation are the base rates and accelerations, while the controlled variables are ω_{Iy} and ω_{Iz}. Substituting (1) into (2) and then into (6), the elevation axis dynamics can then be expressed in terms of the base inputs as

$$J_{Iy}\dot{\omega}_{Iy} + K_{If}\omega_{Iy} + K_{I\omega}\int_0^t \omega_{Iy}(\tau)\,d\tau + \omega_{Iz}\left(\frac{\omega_{Ox} - s_\varepsilon\omega_{Iz}}{c_\varepsilon}\right)(J_{Ix} - J_{Iz}) = T_{Irate} + T_{Ibase} - T_{Uly} - T_{I,\,\mathrm{fric}} - T_{I,\,CR} + K_{If}(c_\eta\omega_{By} - s_\eta\omega_{Bx}) + K_{I\omega}\int_0^t \cdot\,(c_\eta(\tau)\omega_{By}(\tau) - s_\eta(\tau)\omega_{Bx}(\tau))\,d\tau. \tag{8}$$

In a similar manner, the rigid body torque dynamics for the outer gimbal body are derived from

$$\overline{J}_O\dot{\hat{\omega}}(t) + \left(\hat{\omega}_O(t) \times \overline{J}_O\hat{\omega}_O(t)\right) + \left(\hat{L}_I(t)\right)_O = \hat{L}_O(t) \tag{9}$$

where sum of the kinematic torques about the outer gimbal is

$$\hat{L}_O(t) = \begin{bmatrix} T_{Ox}(t) \\ T_{Oy}(t) \\ T_{az}(t) \end{bmatrix} - \begin{bmatrix} T_{UOx}(t) \\ T_{UOy}(t) \\ T_{UOz}(t) \end{bmatrix} - \begin{bmatrix} 0 \\ 0 \\ T_{Of\omega}(t) \end{bmatrix}$$

with

T_{Ox}, T_{Oy}	outer gimbal reaction torques on base;
T_{UOx}, T_{UOy}, T_{UOz}	outer gimbal mass unbalance torques;
T_{az}	azimuth axis stabilization control torque;
$T_{Of\omega}$	friction and cable restraint torque;

$$\left(\hat{L}_I(t)\right)_O = \overline{R}_\varepsilon^T(t)\hat{L}_I(t) = \overline{R}_\varepsilon(t)\left[\overline{J}_I\dot{\hat{\omega}}_I(t) + (\hat{\omega}_I(t) \times J_I\hat{\omega}_I(t))\right]. \tag{10}$$

As with the inner gimbal, alignment is assumed between the principal inertia axes and the axes of rotation, so that the outer inertia matrix is also diagonal. To express the dynamics in terms of the inner body z-axis (cross elevation) one can solve (3) for $\dot{\hat{\omega}}_O$ and substitute the resulting expression and (10) into (9) to obtain

$$\left[\overline{J}_O\overline{R}_\varepsilon^T + \overline{R}_\varepsilon^T\overline{J}_I\right]\dot{\hat{\omega}}_I + (\hat{\omega}_O \times J_O\hat{\omega}_O) + \overline{R}_\varepsilon^T\left(\hat{\omega}_I \times \overline{J}_I\hat{\omega}_I\right) - \overline{J}_O\overline{R}_\varepsilon^T\overline{Q}_\varepsilon\hat{\omega}_O\dot{\varepsilon} - \overline{J}_O\overline{R}_\varepsilon^T\dot{\hat{\varepsilon}} = \hat{L}_O. \tag{11}$$

The cross elevation axis dynamics are generated by the third element of vector (11). Expanding the equation for this component results in

$$c_\varepsilon(J_{Oz} + J_{Iz})\dot{\omega}_{Iz} = s_\varepsilon(J_{Oz} + J_{Ix})\dot{\omega}_{Ix} - \left[\hat{\omega}_O \times \overline{J}_O\hat{\omega}_O - \overline{R}_\varepsilon^T\left(\hat{\omega}_I \times \overline{J}_I\hat{\omega}_I\right)\right]_3 + \left[\overline{J}_O\overline{R}_\varepsilon^T\overline{Q}_\varepsilon\hat{\omega}_O\dot{\varepsilon}\right]_3 + \left[\hat{L}_0\right]_3 \tag{12}$$

where $[\,]_3$ denotes the third element of the vector. Also the last term on the left-hand side of (11) is zero. From (3), the angular acceleration about the inner x-axis can be obtained. Substituting into (12), expanding the cross product terms and substituting the kinematic torques leads to

$$\begin{aligned} J_S\dot{\omega}_{Iz} = {} & s_\varepsilon(J_{Oz} + J_{Ix})\dot{\omega}_{Ox} + (J_{Oz}\omega_{Ix} - s_\varepsilon J_{Ix}\omega_{Oz})\dot{\varepsilon} \\ & - c_\varepsilon[\omega_{Ox}\omega_{Oy}(J_{Oy} - J_{Ox}) - s_\varepsilon\omega_{Iy}\omega_{Iz}J_{Iz} \\ & + \omega_{Iy}\omega_{Ox}J_{Iy} - c_\varepsilon\omega_{Ix}\omega_{Iy}J_{Ix}] \\ & + c_\varepsilon[T_{az} - T_{UOz} - T_{O,\,\mathrm{fric}} - T_{O,\,CR}] \\ & - c_\varepsilon K_{Of}\dot{\eta} - c_\varepsilon K_{O\omega}\eta \end{aligned} \tag{13}$$

where

K_{Of}	outer gimbal viscous friction coefficient;
$K_{O\omega}$	outer gimbal cable restraint coefficient;
J_S	$= J_{Oz} + c_{\varepsilon_\varepsilon}^2 J_{Iz} + s_{\varepsilon_\varepsilon}^2 J_{Ix}$;
T_{az}	$= T_{O\mathrm{rate}} + T_{O\mathrm{base}}$;
$T_{Of\omega}$	$= T_{O,\,\mathrm{fric}} + T_{O,\,CR} + K_{Of}\dot{\eta} + K_{O\omega}\eta$;
$T_{O,\,\mathrm{fric}}$	nonlinear friction torque;
$T_{O,\,CR}$	nonlinear cable restraint torque.

The cross elevation axis dynamics are described by (13). As with the elevation axis, this equation needs to be expressed in terms of the controlled variables ω_{Iz}, ω_{Iy}, the base disturbances $\hat{\omega}_B$, and the elevation and azimuth angles ε and η. The modified expression is derived in Appendix A as

$$\begin{aligned} & J_S\dot{\omega}_{Iz} + K_{Of}\omega_{Iz} + c_\varepsilon K_{O\omega}\int_0^t \frac{1}{c_\varepsilon(\tau)}\,\omega_{Iz}(\tau)\,d\tau \\ & \quad + g_y(t)\omega_{Iy}\omega_{Ox} + g_{yz}(t)\omega_{Iy}\omega_{Iz} = T_{OD\mathrm{base}} + c_\varepsilon \\ & \quad \cdot\left[T_{O\mathrm{rate}} + T_{O\mathrm{base}} - T_{UOz} - T_{O,\,\mathrm{fric}} - T_{O,\,CR}\right]. \end{aligned} \tag{14}$$

The impact of the elevation angle on the cross elevation dynamics is evident from (A2)–(A4). Control of this axis diminishes as the elevation angle increases. A secant gain function can compensate to some degree, however, in practice the gain gets very high for angles beyond 70°. The inability of the two axis system to track through the "cone of occlusion" [4] is commonly termed the NADIR problem.

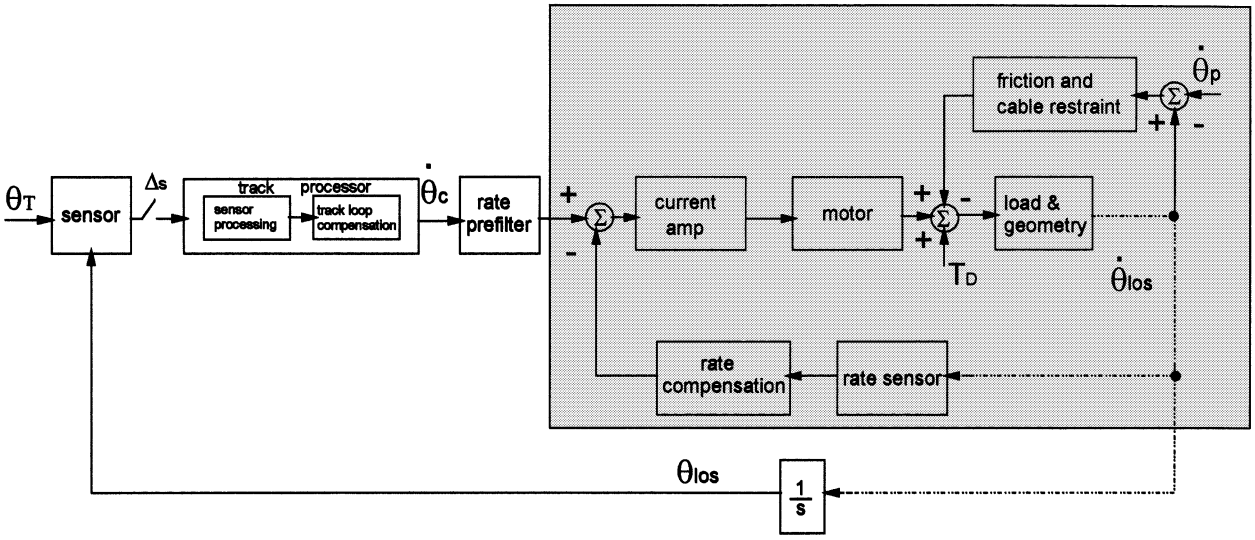

Fig. 2. Control configuration for direct stabilization.

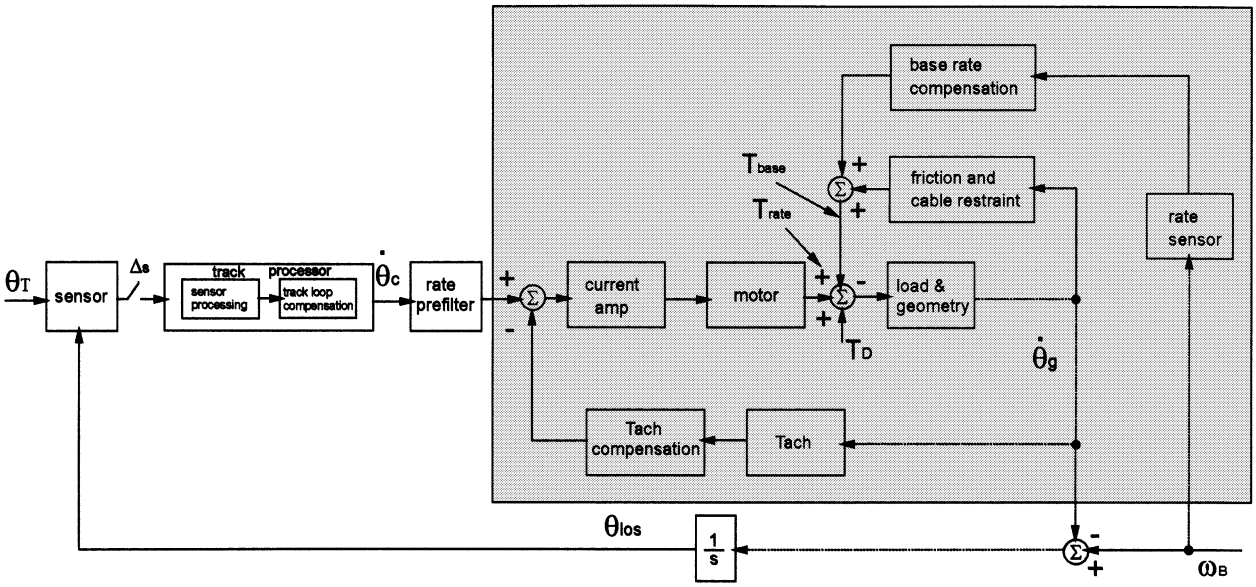

Fig. 3. Control configuration for indirect stabilization.

IV. Stabilization Loop Servo Control

The elevation axis control torque T_{el} and the cross elevation control torque T_{az} can be generated by various algorithms. Regardless of the method, the primary objective is to suppress the effect of any base motion, $\hat{\omega}_B$ (or its derivative). This can be achieved by direct feedback (direct LOS stabilization) and/or disturbance reconstruction and cancellation (indirect LOS stabilization). Significant differences exist between the two approaches, as will be discussed. The control algorithms presented are common practical implementations, derived from classical control methods and bandwidth considerations.

With direct LOS stabilization, a rate sensor measures the rate disturbances ω_{Iy} and ω_{Iz} about the LOS. These are used to generate a feedback compensating torque $T_{I\mathrm{rate}}$, which attempts to null the measured disturbance. The typical control configuration is shown functionally in Fig. 2 for either axis. With indirect stabilization, rate sensors mounted on the base of the gimbal measure platform motion and are used to generate a compensating torque $T_{I\mathrm{base}}$, which attempts disturbance cancellation by matching the measured base rates, transformed into the LOS coordinates, to the LOS disturbance rates. In this method, disturbances induced by relative motion are compensated for by a tachometer feedback loop, which generates a torque $T_{I\mathrm{rate}}$, as in the direct method. The typical control configuration is shown functionally in Fig. 3 for either axis.

A. LOS Stabilization of the Elevation Axis

The elevation axis dynamics were described by (8). With the direct approach a rate sensor mounted on the LOS axes measures ω_{Iy}. To shape the loop response a proportional plus integral (PI) control feedback compensator is often used, or

$$T_{I\mathrm{rate}} = -\left(K_{Py}\omega_{Iym} + K_{Iy}\int_0^t \omega_{Iym}(\tau)\,d\tau\right) \qquad (15)$$

$T_{I\text{base}} = 0$.
$\omega_{Iym} = \omega_{Iy} + \omega_{Iy,\,\text{noise}}$ (measured elevation LOS rate).
$\omega_{Iy,\,\text{noise}}$ Elevation rate sensor measurement error.

The sensor measurement error includes sensor noise. The PI compensator can also be designed to operate on the rate error, which is the difference between the commanded rate from the track loop and the measured rate. In this case the compensator is in the feedforward path, however the results obtained are essentially the same. Substituting the control expression into (8), one obtains

$$\dot{\omega}_{Iy} + \left(\frac{K_{Py} + K_{If}}{J_{Iy}}\right)\omega_{Iy} + \left(\frac{K_{Iy} + K_{I\omega}}{J_{Iy}}\right)\int_0^t \omega_{Iy}(\tau)\,d\tau + \omega_{Iz}\frac{(\omega_{Ox} - s_\varepsilon \omega_{Iz})}{c_\varepsilon}\,\frac{(J_{Ix} - J_{Iz})}{J_{Iy}} = \frac{T_{ID}}{J_{Iy}} + \frac{T_{ID\text{base}}}{J_{Iy}} - \frac{T_{ISN}}{J_{Iy}} \tag{16}$$

where

$T_{ID} = -(T_{UIy} + T_{I,\,\text{fric}} + T_{I,\,CR})$ (inner axis related disturbances);
$T_{ID\text{base}} = K_{If}(c_\eta \omega_{By} - s_\eta \omega_{Bx}) + K_{I\omega}\int_0^t (c_\eta(\tau)\omega_{By}(\tau) - s_\eta(\tau)\omega_{Bx}(\tau))\,d\tau$ (base disturbances);
$T_{ISN} = K_{Py}\omega_{Iy,\,\text{noise}} + K_{Iy}\int_0^t \omega_{Iy,\,\text{noise}}(\tau)\,d\tau$ (sensor noise).

The compensator coefficients are often determined as

$$K_{Py} = 2\pi f_{ry} J_{Iy} - K_{If}; \quad K_{Iy} = (2\pi)^2 f_{ry} f_{ly} J_{Iy} - K_{I\omega}$$

where

f_{ry} elevation rate loop bandwidth;
f_{ly} elevation rate loop lead frequency [$\approx(1/3)f_{ry}$ to $(1/4)f_{ry}$].

Using differential operator notation ($p = d(\cdot)/dt$), (16) can then be expressed as

$$p\omega_{Iy} + 2\pi f_r \omega_{Iy} + (2\pi)^2 f_r f_e \frac{\omega_{Iy}}{p} + \omega_{Iz}\frac{(\omega_{Ox} - s_\varepsilon \omega_{Iz})}{c_\varepsilon}\,\frac{(J_{Ix} - J_{Iz})}{J_{Iy}} = \frac{T_{ID}}{J_{Iy}} + \frac{T_{ID\text{base}}}{J_{Iy}} - \left(\frac{K_{Py}}{J_{Iy}} + \frac{K_{Iy}}{J_{Iy}p}\right)\omega_{Iy,\,\text{noise}}. \tag{17}$$

The elevation axis response is coupled to the cross elevation axis rate and the outer axis roll rate by the fourth term on the left side of (17). In addition, the base rate inputs are also coupled to the azimuth axis response by the relative azimuth angle η. Equation (17) can be rewritten as

$$\omega_{Iy}(t) = \frac{G_{ry}(p)}{J_{Iy}}\left[T_{ID}(t) + T_{ID\text{base}}(t) - \omega_{Iz}\frac{(\omega_{Ox} - s_\varepsilon \omega_{Iz})}{c_\varepsilon}\cdot\frac{(J_{Ix} - J_{Iz})}{J_{Iy}}\right] - \frac{G_{ny}(p)}{J_{Iy}}\,\omega_{Iy,\,\text{noise}}(t) \tag{18}$$

where

$$G_{ry}(p) = \frac{p}{p^2 + 2\pi f_{ry} p + (2\pi)^2 f_{ry} f_{ly}}$$

$$G_{ny}(p) = \frac{K_{Py} p + K_{Iy}}{p^2 + 2\pi f_{ry} p + (2\pi)^2 f_{ry} f_{ly}}.$$

It can be seen that disturbance rejection is derived from the frequency dependent gain (or attenuation factor) $G_{ry}(p)$ and the inertia J_{Iy}. In a point design, f_{ry} and f_{ly} are chosen such that the magnitude of the denominator is sufficient to attenuate a measured torque or acceleration disturbance at a specific frequency(s). The base disturbances are coupled via friction and a cable restraint, but are attenuated by the loop gain. Normally, the desired rate loop bandwidth is such that

$$2\pi f_r \gg \frac{K_{If}}{J_{Iy}} \quad \text{and} \quad (2\pi)^2 f_{ry} f_{ly} \gg \frac{K_{I\omega}}{J_{Iy}}.$$

This essentially results in a high gain feed back approach. It is somewhat robust to parameter variations in the sense that exact knowledge of K_{If}, $K_{I\omega}$, and J_{Iy} is not required as long as the above inequality is satisfied. Sensor noise, however, is only marginally affected by the gain, so that it will still have a significant impact. Sensor noise is coupled via the compensator and will be attenuated (or amplified) roughly as $K_{py}[J_{Iy}(j2\pi f)]^{-1}$. Since disturbance attenuation is inversely proportional to the servo loop bandwidth, it is limited by stability and noise. If the required bandwidth is too high, an alternative algorithm is needed. Identifying the dominant disturbance sources, such as nonlinear friction torque [3], [5], is necessary. In a severe platform motion environment, base sensors can be used to measure ω_{By} and ω_{Bx} and construct a feedback control torque to compensate for the base disturbance input, $T_{ID\text{base}}$ (often termed Strong Stabilization [4]). The basic servo algorithm can be modified to include terms that cancel $T_{I,\,\text{fric}}$, $T_{ID\text{base}}$ (or $T_{I,\,CR}$), and the nonlinear term in ω_{Iz}. This requires the additional measurement of the outer axis roll rate ω_{Ox}.

With the indirect stabilization method, a tachometer is used to measure the relative elevation angular rate $\dot{\varepsilon}$. A tri-axis rate sensor is mounted at the gimbal base to measure $\hat{\omega}_B$. The control torques for this configuration are

$$T_{I\text{rate}} = -\left(K_{Py}\dot{\varepsilon}_m + K_{Iy}\int_0^t \dot{\varepsilon}_m(\tau)\,d\tau\right) \tag{19a}$$

and

$$T_{I\text{base}} = -\left(K_{Py}\omega_{Oy_m} + K_{Iy}\int_0^t \omega_{Oy_m}(\tau)\,d\tau\right) \tag{19b}$$

where

$\omega_{Oy_m} = \omega_{By_m} c_{\eta_m} - \omega_{Bx_m} s_{\eta_m}$ and $\dot{\varepsilon}_m = \dot{\varepsilon} + \dot{\varepsilon}_{\text{noise}}$ measured relative elevation angular rate;
$\dot{\varepsilon}_{\text{noise}}$ elevation tachometer noise;
ω_{By_m}, ω_{Bx_m} measured body y, x rates;
$\omega_{By_m} = \omega_{By} + \omega_{By,\,\text{noise}}$; $\omega_{Bx_m} = \omega_{Bx} + \omega_{Bx,\,\text{noise}}$;
$\eta_m = \eta + \eta_{\text{noise}}$ (measured resolver angle);
$c_{\eta_m} = \cos(\eta_m)$; $s_{\eta_m} = \sin(\eta_m)$;
η_{noise} azimuth resolver noise.

It is also likely that the command for the compensation torque, $T_{I\text{base}}$, will be computer generated and contain sampling errors associated with the base rate sensor and resolver measurements. For a fast enough sampling rate, this error component will be proportional to the sampling interval, Δ This analysis, ignores this source of error and treats the command

torque as an analog signal. Expanding the expression for ω_{0y_m} and assuming the resolver error is small results in

$$\omega_{Oy_m} = \omega_{Oy} + \omega_{Oy,\,\mathrm{noise}}$$

where

$$\omega_{Oy,\,\mathrm{noise}} = -(\omega_{Ox}\eta_{\mathrm{noise}} - (\omega_{By,\,\mathrm{noise}}c_\eta - \omega_{Bx,\,\mathrm{noise}}s_\eta) - \eta_{\mathrm{noise}}(\omega_{Bx,\,\mathrm{noise}}c_\eta - \omega_{By,\,\mathrm{noise}}s_\eta)).$$

The combined inner gimbal compensation torques are then obtained as

$$T_{I\mathrm{rate}} + T_{I\mathrm{base}} = -\left(K_{Py}\omega_{Iy} + K_{Iy}\int_0^t \omega_{Iy}(\tau)\,d\tau\right) - K_{Py}\left(\dot{\varepsilon}_{\mathrm{noise}} + \omega_{Oy,\,\mathrm{noise}}\right) - K_{Iy}\int_0^t \cdot\left(\dot{\varepsilon}_{\mathrm{noise}}(\tau) + \omega_{Oy,\,\mathrm{noise}}(\tau)\right)d\tau. \quad (20)$$

Substituting (19) into (8), and using the same algorithm to choose the servo loop compensator coefficients as described in Section IV-A, one has

$$\omega'_{Iy}(t) = \frac{G_{ry}(p)}{J_{Iy}}\left[T_{ID}(t) + T_{ID\mathrm{base}}(t) - \omega_{Iz}\frac{(\omega_{Ox} - s_\varepsilon\omega_{Iz})}{c_\varepsilon}\,\frac{(J_{Ix} - J_{Iz})}{J_{Iy}}\right] - \frac{G_{ny}(p)}{J_{Iy}}\left(\dot{\varepsilon}_{\mathrm{noise}}(t) + \omega_{Oy,\,\mathrm{noise}}(t)\right). \quad (21)$$

Comparison of (18) with (21), indicates that the loop gain for both approaches will be equivalent. The major difference is in the noise terms. Whereas the direct approach contains only the elevation rate sensor noise, the indirect approach is perturbed by both tachometer noise as well as base rate sensor noise. The difference in the noise terms arises from a fundamental difference in the control technique. The direct approach suppresses the disturbances via gain attenuation. The disturbance is never totally applied to the rate loop since it is always working to null it. Its magnitude as seen by the loop, is dependent on the loop bandwidth. The indirect approach requires a cancellation of the rate ω_{0y} so that it must actually be measured. To estimate performance of the two approaches, one can compare the root mean square (rss) rate sensor error $\omega_{Iy,\,\mathrm{noise}}$ of the direct LOS method with an estimate of the indirect LOS method noise as given by the root sum square (rss) of the rms noise of the tachometer, resolver, and base rate sensors, or

$$\sqrt{\dot{\varepsilon}^2_{\mathrm{noise}} + (\eta_{\mathrm{noise}}\omega_{Ox})^2 + \omega^2_{Bx,\,\mathrm{noise}} + \omega^2_{By,\,\mathrm{noise}}}.$$

It is important to note that a noise contribution from the azimuth resolver, dependent on the outer gimbal axis roll rate, now impacts the elevation axis performance. Indirect method performance could be improved by mounting a rate sensor on the outer gimbal to measure ω_{Oy} directly.

B. LOS Stabilization of the Cross-Elevation Axis

The cross elevation axis dynamics were described by (14). With the direct approach the cross elevation rate ω_{Iz} is measured directly and fed back to suppress disturbances about this axis. Again, a simple proportional plus integral control compensator is used, or

$$T_{O\mathrm{rate}} = -\left(K_{Pz}\omega_{Iz_m} + K_{Iz}\int_0^t \omega_{Iz_m}(\tau)\,d\tau\right)$$
$$T_{O\mathrm{base}} = 0 \quad (22)$$

where

ω_{Iz_m} $= \omega_{Iz} + \omega_{Iz,\,\mathrm{noise}}$ measured cross-elevation rate.
$\omega_{IZ,\,\mathrm{noise}}$ cross-elevation rate sensor measurement error.

As with the elevation axis, the sensor measurement error includes noise. Substituting (22) into (14), and restricting the analysis to small elevation angles, then

$$\dot{\omega}_{Iz} + \left(\frac{K_{Of}}{J_S} + \frac{K_{Pz}}{J_S}\right)\omega_{Iz} + \left(\frac{K_{O\omega}}{J_S} + \frac{K_{Iz}}{J_S}\right)\int_0^t \omega_{Iz}(\tau)\,d\tau + \frac{g_y(t)\omega_{Ox}}{J_S}\,\omega_{Iy} + \frac{g_{yz}(t)}{J_S}\,\omega_{Iy}\omega_{Iz} = \frac{T_{OD\mathrm{base}}}{J_S} + \frac{T_{OD}}{J_S} - \frac{T_{OSN}}{J_S} \quad (23)$$

where

T_{OD} $= -(T_{O,\,\mathrm{fric}} + T_{O,\,CR} + T_{UOz})$.
T_{OSN} $= K_{Pz}\omega_{Iz,\,\mathrm{noise}} + K_{Iz}\int_0^t \omega_{Iz,\,\mathrm{noise}}(\tau)\,d\tau$ sensor noise.

The PI coefficients are chosen using the same algorithm as for the elevation axis (f_{rz} and f_{lz} are again the loop bandwidth and lead frequency), or

$$K_{Pz} = 2\pi f_{rz}J_S - K_{Of} \quad \text{and} \quad K_{Iy} = (2\pi)^2 f_{rz}f_{lz}J_S - K_{O\omega}.$$

The cross-elevation response is then approximated as

$$\omega_{Iz} = \frac{G_{rz}(p)}{J'_S}\left[T_{OD\mathrm{base}}(t) + T_{OD}(t) - g_y(t)\omega_{Ox}\omega_{Iy} - g_{yz}(t)\omega_{Iy}\omega_{Iz}\right] - \frac{G_{nz}(p)}{J'_S}\,\omega_{Iz,\,\mathrm{noise}} \quad (24)$$

where

$$G_{rz}(p) = \frac{p}{p^2 + 2\pi f_{rz}p + (2\pi)^2 f_{rz}f_{lz}}$$
$$G_{nz}(p) = \frac{K_{Pz}p + K_{Iz}}{p^2 + 2\pi f_{rz}p + (2\pi)^2 f_{rz}f_{lz}}$$

and $J'_S \sim J_{Oz} + J_{Iz}$. With these approximations, rate loop performance depends upon loop gain and axis inertia, as with the elevation axis. Again, coupling of this axis with the elevation axis is seen to be dependent upon the outer axis roll rate.

The indirect stabilization control configuration again includes a tachometer to measure the relative azimuth angular rate, $\dot{\eta}$, and the tri-axis rate sensor, specified previously, mounted on the gimbal base. The control torques for this case are given by

$$T_{O\mathrm{rate}} = -\left(K_{Pz}\dot{\eta}_m + K_{Iz}\int_0^t \dot{\eta}_m(\tau)\,d\tau\right) \quad (25a)$$

$$T_{O\mathrm{base}} = -\left(K_{Pz}\left(\omega_{Ox_m}\tan\varepsilon_m + \omega_{Bz_m}\right) + K_{Iz}\int_0^t \cdot\left(\omega_{Ox_m}(\tau)\tan\varepsilon_m(\tau) + \omega_{Bz_m}(\tau)\right)d\tau\right) \quad (25b)$$

$$\omega_{Ox_m} = \omega_{Bx_m}c_{\eta_m} + \omega_{By_m}s_{\eta_m}$$

where

ε_m measured relative elevation axis angle;

$\varepsilon_m = \varepsilon + \varepsilon_{\text{noise}}$; $\omega_{Bz_m} = \omega_{Bz} + \omega_{Bz,\,\text{noise}}$.

Again, issues regarding the base torque being computer generated and having an associated sampling error will be ignored. The expression for the rate ω_{Ox_m} can be expanded (again assuming the resolver errors are small) as

$$\omega_{Ox_m} = \omega_{Ox} + \omega_{Ox,\,\text{noise}}$$

where

$$\omega_{Ox,\,\text{noise}} = \omega_{Oy}\eta_{\text{noise}} + (\omega_{Bx,\,\text{noise}}c_\eta + \omega_{Bx,\,\text{noise}}s_\eta) - \eta_{\text{noise}}(\omega_{Bx,\,\text{noise}}s_\eta + \omega_{By,\,\text{noise}}c_\eta).$$

For small elevation angles, $\tan(\varepsilon_m)$ in (25b) can be approximated as $\tan(\varepsilon_m) \sim \tan(\varepsilon) + \varepsilon_m$ and the base control torque can be expressed as

$$\begin{aligned} T_{Obase} = &-\Big(K_{Pz}(\omega_{Ox}\tan\varepsilon + \omega_{Bz}) + K_{Iz}\int_0^t \cdot(\omega_{Ox}(\tau)\tan\varepsilon(\tau) + \omega_{Bz}(\tau))\,d\tau\Big) \\ &-\Big(K_{Pz}(\omega_{Ox,\,\text{noise}}\tan\varepsilon_m + \omega_{Ox}\varepsilon_{\text{noise}} - \omega_{Bz,\,\text{noise}}) \\ &+ K_{Iz}\int_0^t (\omega_{Ox,\,\text{noise}}(\tau)\tan\varepsilon_m(\tau) + \omega_{Ox}(\tau) \cdot\varepsilon_{noise}(\tau) + \omega_{Bz,\,\text{noise}}(\tau))\,d\tau\Big). \end{aligned} \tag{26}$$

The combined outer gimbal azimuth compensation torque can finally be generated as

$$\begin{aligned} T_{O\text{rate}} + T_{O\text{base}} = &-\left(K_{Pz}\frac{\omega_{Iz}}{c_\varepsilon} + K_{Iz}\int_0^t \frac{\omega_{Iz}(\tau)}{c_\varepsilon(\tau)}\,d\tau\right) \\ &-\left(K_{Pz}e_{\eta z} + K_{Iz}\int_0^t e_{\eta z}(\tau)\,d\tau\right) \end{aligned} \tag{27}$$

where $e_{\eta z} = \dot{\eta}_{\text{noise}} - \omega_{Ox,\,\text{noise}}\tan\varepsilon_m + \omega_{Ox}\varepsilon_{\text{noise}} + \omega_{Bz,\,\text{noise}}$. Substituting (27) into (14), one obtains

$$\begin{aligned} &\dot{\omega}_{Iz} + \left(\frac{K_{Of}}{J_S} + \frac{K_{Pz}}{J_S}\right)\omega_{Iz} \\ &\quad + c_\varepsilon\left[\left(\frac{K_{O\omega}}{J_S} + \frac{K_{Iz}}{J_S}\right)\int_0^t \frac{\omega_{Iz}(\tau)}{c_\varepsilon(\tau)}\,d\tau\right] \\ &\quad + \frac{g_y(t)}{J_S}\omega_{Iy}\omega_{Ox} + \frac{g_{yz}(t)}{J_S}\omega_{Iy}\omega_{Iz} \\ &\quad = \frac{T_{OD\text{base}}}{J_S} + \frac{c_\varepsilon}{J_S}(T_{OD} - T_{OSN}) \end{aligned}$$

where

$$T_{OSN} = K_{Pz}e_{\eta z} + K_{Iz}\int_0^t e_{\eta z}(\tau)\,d\tau. \tag{28}$$

With the small elevation angle assumption, the response can be approximated as

$$\begin{aligned} \omega_{Iz}(t) = \frac{G_{rz}(p)}{J_S'}\,[&T_{OD\text{base}}(t) + T_{OD}(t) - g_y(t)\omega_{Ox}\omega_{Iy} \\ &- g_{yz}(t)\omega_{Iy}\omega_{Iz}] - \frac{G_{nz}(p)}{J_S'}\,(e_{\eta z}(t)). \end{aligned} \tag{29}$$

The transfer functions G_{rz} and G_{nz} are similar to those defined for the elevation axis. The primary difference between the direct and indirect approaches is again the noise term. The rate sensor noise, $\omega_{Iz,\,\text{noise}}$, can be compared with an upper bound of the rss of the rms noise associated with the indirect approach, or $\sqrt{\dot{\eta}^2_{\text{noise}} + \omega^2_{Ox,\,\text{noise}} + (\varepsilon_{\text{noise}}\omega_{Ox})^2 + \omega^2_{Bz,\,\text{noise}}}$ where the rms of $\omega_{Ox,\,\text{noise}}$ is approximated as shown in the equation at the bottom of the page.

Again the dependence of the rms noise on the resolver angle noise contribution and the outer axis roll and pitch rates can be observed. As with the elevation axis, in the presence of bandwidth limitations, enhanced performance may be possible by canceling the terms associated with $g_y(t)$ and $g_{yz}(t)$ as well as direct compensation of friction and cable restraint torques.

C. General Stabilization Servo Loop Requirements

The preceding stabilization loop analysis focused on specific control algorithms based on known design techniques. More insight into stabilization loop design requirements may be obtained by formulating the problem in a general structure. The models describing the gimbal dynamics for the elevation and cross elevation axes, given by (8) (EL) and (14) (Cross EL), can be expressed in a differential vector form as

$$\dot{\hat{X}} = \overline{A}(t)\hat{X}(t) + \hat{F}\left(\hat{X},\,t\right) + \overline{J}^{-1}\left[\hat{T}_{\text{rate}} + \hat{T}_{\text{base}} + \hat{T}_{\text{dist}}\right] \tag{30}$$

where

$$x_1(t) = \int_0^t \omega_{Iy}(t)\,dt; \qquad \dot{x}_1(t) = x_2(t) = \omega_{Iy}(t);$$

$$x_3(t) = \int_0^t \omega_{Iz}(\tau)\,d\tau; \qquad \dot{x}_3(t) = x_4(t) = \omega_{Iz}(t)$$

$$\hat{F}\left(\hat{X},\,t\right)^T = \left[0,\, J_{\Delta z}\omega^2_{Iz}\tan(\varepsilon),\, 0,\, \frac{g_{yz}(t)\omega_{Iy}\omega_{Iz}}{J_S}\right]$$

$$J_{\Delta z} = \frac{J_{Ix} - J_{Iz}}{J_{Iy}}$$

$$\sqrt{(\eta_{\text{noise}}\omega_{Oy})^2 + \omega^2_{By,\,\text{noise}} + \omega^2_{Bx,\,\text{noise}} + \eta^2_{\text{noise}}\left(\omega^2_{Bx,\,\text{noise}} + \omega^2_{By,\,\text{noise}}\right)}.$$

and

$$T_{I\text{dist}} = -T_{UIy} - T_{I,\text{fric}} - T_{I,CR} + T_{ID\text{base}}$$

$$T_{Odist} = -T_{UOy} - T_{O,\text{fric}} - T_{O,CR} + T_{ODbase}$$

$$\hat{T}^T_{\text{rate}} = [0,\, T_{I\text{rate}},\, 0,\, T_{O\text{rate}}]$$

$$\hat{T}^T_{\text{base}} = [0,\, T_{I\text{base}},\, 0,\, T_{O\text{base}}]$$

$$\hat{T}^T_{O\text{dist}} = [0,\, T_{I\text{dist}},\, 0,\, T_{O\text{dist}}]$$

$$\overline{J}^{-1} = \begin{bmatrix} 0 & 0 & 0 & 0 \\ 0 & J_{Iy}^{-1} & 0 & 0 \\ 0 & 0 & 0 & 0 \\ 0 & 0 & 0 & J_S^{-1} \end{bmatrix}$$

$$\overline{A}(t) = \begin{bmatrix} 0 & 1 & 0 & 0 \\ \dfrac{-K_{I\omega}}{J_{Iy}} & \dfrac{-K_{If}}{J_{Iy}} & 0 & -J_{\Delta z}\omega_{Ox} \\ 0 & 0 & 0 & 1 \\ 0 & \dfrac{-g_y(t)\omega_{Ox}}{J_S} & \dfrac{-K_{O\omega}}{J_S} & \dfrac{-K_{Of}}{J_S} \end{bmatrix}.$$

The direct LOS stabilization feedback design produces a control torque given by

$$\hat{T}_{\text{rate}} = -\overline{D}\hat{X}; \qquad \hat{T}_{\text{base}} = 0 \tag{31}$$

where $\overline{D}$ is given in the equation at the bottom of the page. Substituting (31) into (30), one obtains

$$\dot{\hat{X}} = \overline{A}_O(t)X(t) + \hat{F}\left(\hat{X},\, t\right) + J^{-1}\hat{T}_{\text{dist}} \tag{32}$$

where

$$\overline{A}_O(t) = \overline{A}(t) - \overline{J}^{-1}\overline{D}$$

or

$$\overline{A}_O(t) = \begin{bmatrix} 0 & 1 & 0 & 0 \\ -(2\pi)^2 f_{ry} f_{ly} & -2\pi f_{ry} & 0 & -(J_{\Delta z})\omega_{Ox} \\ 0 & 0 & 0 & 1 \\ 0 & -\dfrac{g_y(t)\omega_{Ox}}{J_S} & -(2\pi)^2 f_{rz} f_{lz} & -2\pi f_{rz} \end{bmatrix}.$$

Equation (32) represents the gimbal response to a disturbance input vector for the direct LOS stabilization approach. The servo loop gains, which attenuate the input disturbance, are now inherent in the matrix $\overline{A}_0(t)$. A similar expression can be derived for the indirect LOS stabilization case. As suggested earlier to improve performance, a strong stabilization approach [4] might be utilized in which case the feedback and base torques could be modified as $\hat{T}_{\text{rate}} = \overline{D}\hat{X} - \overline{J}\hat{F}_e(\hat{X},\, t)$; $\hat{T}_{\text{base}} = -\hat{T}_{\text{dist},\, e}$ where $\hat{F}_e(\hat{X},\, t)$ is an estimate of the nonlinear feedback vector and $\hat{T}_{\text{dist},\, e}$ the estimated base disturbance input. With these control inputs, the response becomes

$$\dot{\hat{X}} = \overline{A}_O(t)\hat{X} + \Delta\hat{F}(X,\, t) + \overline{J}^{-1}\,\Delta\hat{T}_{\text{dist}}$$

where

$$\Delta\hat{F}(X,\, t) = \hat{F}\left(\hat{X},\, t\right) - \hat{F}_e\left(\hat{X},\, t\right)$$

and

$$\Delta\hat{T}_{\text{dist}} = \hat{T}_{\text{dist}} - \hat{T}_{\text{dist},\, e}.$$

The difference vectors are the residual errors resulting from the cancellation of the respective terms. Implementation of the base disturbance cancellation torque requires knowledge of the base rates, gimbal inertia, linear friction and cable restraint constants, and gimbal angles as well as a model of the nonlinear friction torque [5], [6].

Another stability measure for the feedback design can be obtained by examining the linear part of the response to determine conditions under which the $\overline{A}_0(t)$ matrix eigenvalues have negative real parts. A first-order estimate of the feedback gain requirements can be obtained by treating the time varying terms of $\overline{A}_0(t)$ as constants. The characteristic equation is then given by

$$\left(s^2 + 2\pi f_{ry}s + (2\pi)^2 f_{ry}f_{ly}\right)\left(s^2 + 2\pi f_{rz}s + (2\pi)^2 f_{rz}f_{lz}\right) - \frac{g_y J_{\Delta z}}{J_S}\,\omega_{Ox}^2 s^2 = 0.$$

Using the Routh criterion to establish stability conditions, a quick estimate can be had by assuming that the bandwidths and lead frequencies of each loop are equal, or

$$\left(s^2 + 2\pi f_r s + (2\pi)^2 f_r f_l\right)^2 = \frac{g_y J_{\Delta z}}{J_S}\,\omega_{Ox}^2 s^2.$$

With this assumption, it can be shown that the following stability condition results:

$$2\pi f_r > \left\{\sqrt{\frac{g_y J_{\Delta z}}{J_S}\,\omega_{Ox}}\right\}_{\max}.$$

$$\overline{D} = \begin{bmatrix} 0 & 0 & 0 & 0 \\ (2\pi)^2 f_{ry} f_{ly} J_{Iy} - K_{I\omega} & 2\pi f_{ry} J_{Iy} - K_{If} & 0 & 0 \\ 0 & 0 & 0 & 0 \\ 0 & 0 & (2\pi)^2 f_{rz} f_{lz} J_S - K_{O\omega} & 2\pi f_{rz} J_S - K_{Of} \end{bmatrix}$$

This lower bound on loop bandwidth indicates it must exceed a value dependent upon the inertia terms and the maximum expected roll rate, assuming ε is small and the term $g_y(t)$ (see Appendix A) is bounded. Conditions under which the solution to the homogenous part of (32) approaches zero as time tends to infinity can also be derived directly from the state-space representation. The matrix $\overline{A}_0(t)$ can be expressed as: $\overline{A}_O(t) = \overline{A}_O + \overline{\delta A}_O(t)$ where $\overline{A}_O$ contains only the constant elements and eigenvalues with negative real parts and $\overline{\delta A}_O(t)$ contains the two time varying roll elements (element 2,4 and element 4,2). Equation (32) can then be written as ($\hat{T}_{\text{dist}} = 0$)

$$\dot{\hat{X}}(t) = \overline{A}_O \hat{X}(t) + \overline{\delta A}_O(t)\hat{X}(t) + \hat{F}\left(\hat{X},\, t\right). \tag{33}$$

This vector equation has the solution

$$\hat{X}(t) = \text{EXP}\left(\overline{A}_O t\right)\hat{X}(0) + \int_0^t \text{EXP}\left(\overline{A}_O(t-\tau)\right) \cdot \left(\overline{\delta A}_O(\tau)\hat{X}(\tau) + \hat{F}\left(\hat{X},\, \tau\right)\right) d\tau \tag{34}$$

where $\text{EXP}(\overline{A}_O t)$ is the state transition matrix. The following positive bounds are assumed:

$$\left\|\hat{X}(0)\right\| \le K_O; \qquad \left\|\text{EXP}\left(\overline{A}_O t\right)\right\| \le \beta e^{-\lambda t}$$

$$\left\|\overline{\delta A}_O(t)\right\| \le K_J|\omega_{Ox}|_{\max}; \qquad K_J \propto \left\{\sqrt{\frac{g_y^2}{J_S^2} + J_{\Delta z}^2}\right\}_{\max}.$$

The nonlinear term $\hat{F}$ is a product of the state variables. For ε small, it will satisfy the following condition [$J_{\max}$ is a maximum value of the inertia terms associated with $F(X,\, t)$]

$$\lim_{x\to 0} \frac{\left\|\hat{F}\left(\hat{X},\, t\right)\right\|}{\left\|\hat{X}(t)\right\|} \to 0$$

since

$$\left\|\frac{F\left(\hat{X},\, t\right)}{\hat{X}(t)}\right\| \le \frac{\varepsilon\omega_{Iz} J_{\max}\sqrt{\omega_{Iz}^2 + \omega_{Iy}^2}}{\left\|\hat{X}(t)\right\|} \le \varepsilon\omega_{Iz} J_{\max}.$$

Therefore, for $\|X(\tau)\| \le \delta$ and $t > t_0$ the following condition will be met: $\|F(\hat{X},\, t)\| \le K_F\|X\|$. This bound on the state vector norm is dependent on the initial state vector. Taking the norm of both sides of (34), one has

$$\ell(t) \le \beta K_O e^{-\lambda t} + \int_0^t \beta e^{-\lambda(t-\tau)}\left(\left(K_J|\omega_{Ox}|_{\max} + K_F\right)\ell(\tau)\right) d\tau \tag{35}$$

where $\ell(t) = \|\hat{X}(t)\|$ assuming that

$$\|X(\tau)\| \le \delta \qquad \text{for } t_0 \le \tau \le t.$$

It is shown in Appendix B, that this bound can be expressed as: $\ell(t) \le \beta K_O e^{-(\lambda - (K_J|\omega_{Ox}|_{\max} + K_F)\beta)t}$. If the roll rate is bounded such that $(K_J|\omega_{Ox}|_{\max} + K_F) < \lambda/\beta$, then the state vector norm is exponentially decaying. To satisfy the condition that $\|X(\tau)\| \le [\delta$ for $t_0 \le [\tau < [t$ and all $t\ \mu\ t_0$, it is necessary to select K_O such that

$$K_O \le \frac{\delta}{\beta} e^{(\lambda - (K_J|\omega_{Ox}|_{\max} + K_F)\beta)t}$$

or

$$K_O \le \frac{\delta}{\beta} \qquad \text{for } \frac{\lambda}{\beta} = K_J|\omega_{Ox}|_{\max} + K_f.$$

The bound is a function of the initial state, due to the nonlinear feedback term. Although the practical significance of this result may be limited, it does provide some insight into the lower bound on the loop bandwidth and gain required for a reasonably stable response.

TABLE I

	Case One	Case Two	Case Three
ω_{Bx} (rad/sec)	2.5	0.16	0.06
F_{Bx} (Hz)	1	1	1
ω_{By} (rad/sec)	0.185	0.05	0.1
F_{By} (Hz)	1.5	1	2
ω_{Bz} (rad/sec)	0.103	0.1	0.1
F_{Bz} (Hz)	2	1	2

V. Simulation

The gimbal model derived in previous sections and defined by (8) and (14), was simulated in order to provide a quantitative comparison of the two stabilization methods. The gimbal parameters assumed were the following.

Inner Axis Inertia:

$J_{Ix} = 0.05$ lb-in-s^2; $J_{Iy} = 0.325$ lb-in-s^2; $J_{Iz} = 0.2$ lb-in-s^2

Inner and Outer Axis Friction:

(viscous) K_{If}, $K_{Of} = 0.56$ lb-in/rad/s;

(Coulomb) $T_{I,\,\text{fric}}$, $T_{O,\,\text{fric}} = 0.75$ lb-in/rad/s

inner and outer axis cable restraint:

$K_{I\omega}$, $K_{O\omega} = 0.1$ lb-in/rad

outer axis inertia:

$J_{Ox} = 0.1$ lb-in-s^2; $J_{Oy} = 0.4$ lb-in-s^2; $J_{Oz} = 0.6$ lb-in-s^2.

A 30-Hz servo bandwidth was obtained on the inner (elevation) axis and an approximate 20 Hz bandwidth on the outer (cross elevation) axis using a PI compensator given by

$$G_C(s) = 180\,\frac{(s+25)}{s}.$$

Three cases were simulated, representative of different platform types, with the following sinusoidal disturbance rates [i.e., $\omega_{dist} = \omega_B \sin(2\pi f_B t)$] as listed in Table I.

The rate sensor noise was assumed to be normally distributed with a zero mean and a standard deviation of 0.005 rad/s. The resolver noise was also assumed zero mean normal with a standard deviation of 0.001 rad. Sampling of the resolver angles was not modeled so that this source of error is not included.

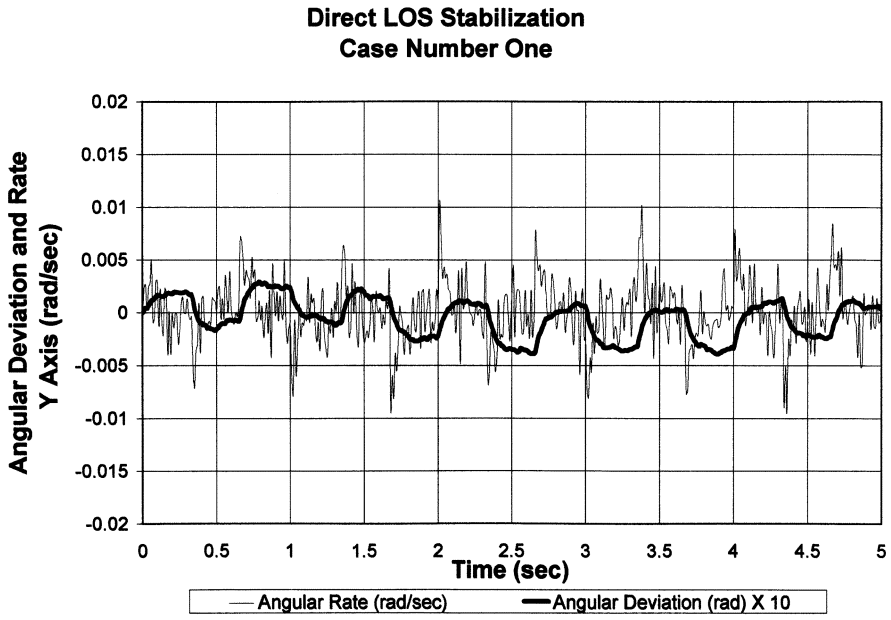

Fig. 4. Direct LOS stabilization Case One.

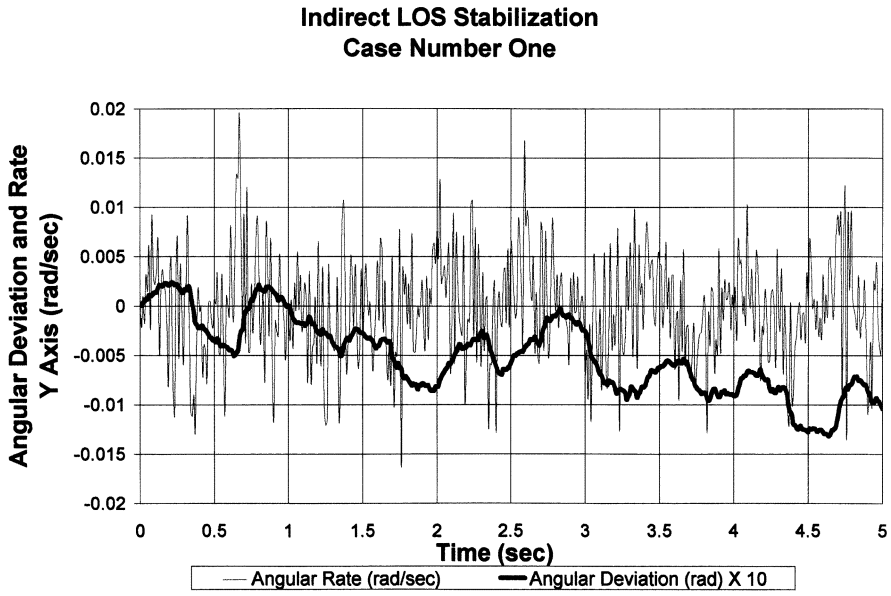

Fig. 5. Indirect LOS stabilization Case One.

The simulation results for Case One, representing a severe disturbance environment (with a significant platform roll rate), are shown in Figs. 4–6. Fig. 4 is a plot of the LOS angular and rate disturbance about the inner axis for the direct approach. Fig. 5 is the same plot, but for the indirect approach. Comparing the rate disturbances for each approach, it is evident that the density of the variations observed with the indirect approach is higher than for the direct approach. The disturbance rate distribution is plotted in Fig. 6 to quantify this observation. It can be seen that for the indirect approach, the distribution has a much broader spectrum than for the direct approach. This supports the analysis that indicated more error sources were associated with the indirect approach. Similar results were obtained for the outer axis. Figs. 4 and 5 also show the LOS angular deviation. With the indirect approach, the drift in the deviation due to the low frequency rate bias resulting from the composite rate disturbances, such as the integrated roll/resolver error disturbance product [see (28)], is much higher. The inner axis disturbance rate distribution plot for Case Two is shown in Fig. 7. The average amplitude of the rate disturbances for this case is lower than for Case One, however, the same trends can be observed. The disturbance distribution resulting from the indirect control method is again significantly greater than with the direct method. Again similar results were obtained for the outer axis. The final case represents very low disturbance conditions with a correspondingly low roll rate. The rate distribution plot for the inner axis is shown in Fig. 8 and again the trend is similar to the previous two cases.

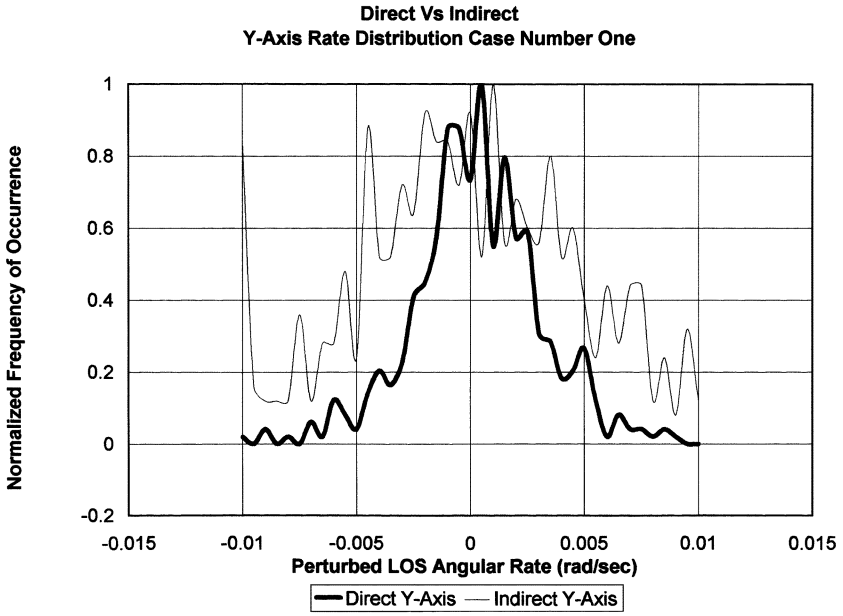

Fig. 6. Y-axis rate distribution Case One.

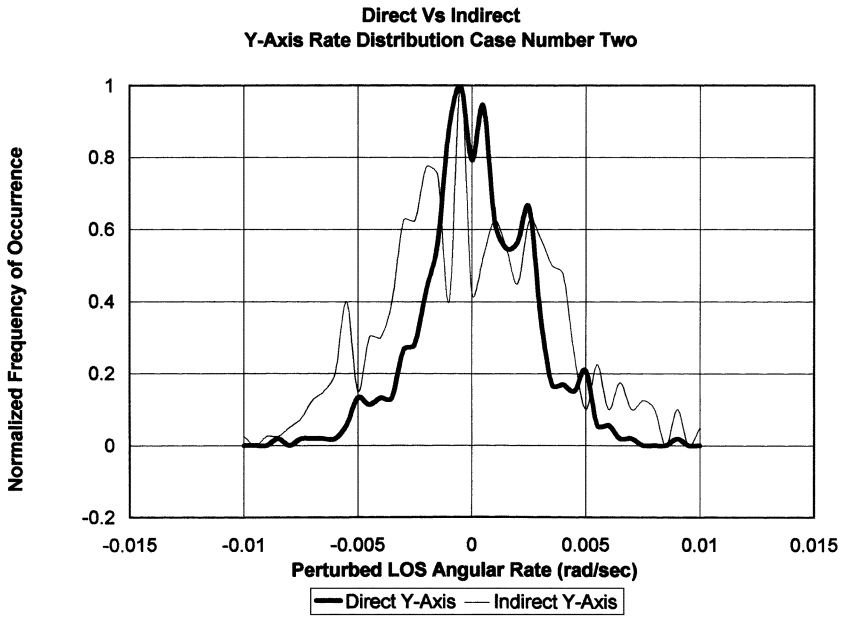

Fig. 7. Y-axis rate distribution Case Two.

VI. Summary

A two-axis gimbal model was derived to evaluate the performance of two methods for stabilizing the LOS pointing vector. With the direct approach, the rate sensors are mounted on the LOS axes and directly measure rate disturbances about the elevation and cross-elevation axes. With the indirect approach, the rate sensors are mounted at the gimbal base, and compensation requires that these rates be transformed into equivalent disturbances about the LOS. In this approach, relative rate disturbances such as friction, and imbalance are compensated for by tachometer feedback about the torque motor. The analysis showed that more error sources were associated with the indirect approach. The simulation results verified this and indicated that the performance of the indirect approach would not be as efficient as with the direct approach. In the indirect approach, several of the noise inputs are coupled to the platform roll disturbance. For both methods, it was shown that a lower bound on stabilization loop bandwidth was proportional to the maximum expected roll rate disturbance, coupled in via gimbal geometry. The analysis of the indirect method did not account for sampling rate errors or those associated with the gimbal structural rigidity. Essentially, all signals were assumed to be analog. Before choosing a particular method, one must tradeoff the advantage gained with the indirect approach from the payload volume reduction versus the penalty paid in LOS disturbance attenuation performance. Although, indirect LOS stabilization performance may be satisfactory, this approach will not attain the same performance level as the direct approach, given an equal design effort.

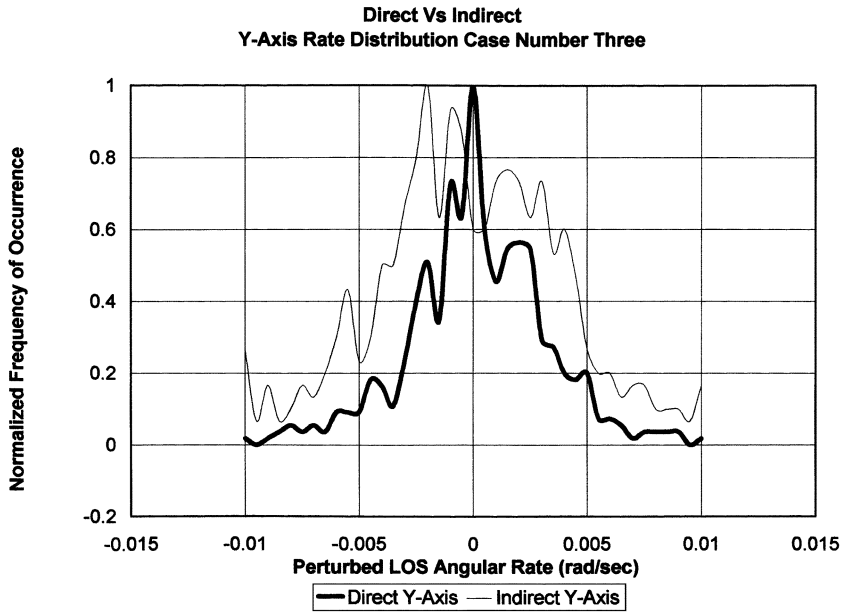

Fig. 8. Y-axis rate distribution Case Three.

APPENDIX A

Equation (13), given in Section III, can be modified by expressing the variables ω_{Ix} and ω_{0z} in terms of the controlled variables and base disturbances. The following expressions for ω_{Ix} and ω_{0z} are used to generate this representation:

$$\omega_{Ix} = \frac{1}{c_\varepsilon}(\omega_{Ox} - s_\varepsilon \omega_{Iz}); \qquad \omega_{Oz} = \frac{1}{c_e}(\omega_{Iz} - s_\varepsilon \omega_{Ox}).$$

Using these equations, the first term on the right-hand side of (13) can be expressed as

$$s_\varepsilon(J_{Oz}+J_{Ix})\left[\dot{\omega}_{Bx}c_\eta - \dot{\omega}_{By}s_\eta + \omega_{Oy}\omega_{Ox}\tan\varepsilon + \omega_{Oy}\omega_{Bz}\right] - (J_{Oz}+J_{Ix})\omega_{Iz}\omega_{Iy}\tan\varepsilon$$

the second term as

$$(J_{Oz}+J_{Ix})\omega_{Oy}\omega_{Oz}\tan\varepsilon - (J_{Oz}+J_{Ix})\omega_{Iz}\omega_{Iy}\tan\varepsilon + \frac{1}{c_\varepsilon}\left(J_{Oz}+s_\varepsilon^2 J_{Ix}\right)\omega_{Ox}\omega_{Iy} - \frac{1}{c_\varepsilon}\left(J_{Oz}+s_\varepsilon^2 J_{Ix}\right)\omega_{Ox}\omega_{Oy}$$

the third term as

$$c_\varepsilon\omega_{Ox}\omega_{Iy}(J_{Iy}-J_{Ix}) - c_\varepsilon s_\varepsilon\omega_{Iy}\omega_{Iz}(J_{Iz}-J_{Ix}) + c_\varepsilon\omega_{Ox}\omega_{Oy}(J_{Oy}-J_{Ox})$$

and finally, the friction and cable restraint term as

$$c_\varepsilon K_{Of}\dot{\eta} = K_{Of}\omega_{Iz} - K_{Of}s_\varepsilon\omega_{Ox} - K_{Of}c_\varepsilon\omega_{Bz}$$

$$c_\varepsilon K_{O\omega}\eta = c_\varepsilon K_{O\omega}\int_0^t \left(\frac{1}{c_\varepsilon(\tau)}(\omega_{Iz}(\tau) - s_\varepsilon(\tau)\omega_{Ox}(\tau)) - \omega_{Bz}(\tau)\right)d\tau.$$

Substituting each of these expressions into (13) results in the following representation for the cross elevation dynamics:

$$\begin{aligned} J_S\dot{\omega}_{Iz} &+ K_{Of}\omega_{Iz} + c_\varepsilon K_{O\omega}\int_0^t \frac{1}{c_\varepsilon(\tau)}\omega_{Iz}(\tau)\,d\tau \\ &+ g_y(t)\omega_{Ox}\omega_{Iy} + g_{yz}(t)\omega_{Iy}\omega_{Iz} \\ &= T_{O\text{base}} + c_\varepsilon[T_{Orate} + T_{O\text{base}} - T_{UOz} - T_{O,\text{fric}} - T_{O,CR}] \end{aligned} \tag{A1}$$

where

$$\begin{aligned} T_{O\text{base}} = {} & s_\varepsilon(J_{Oz}+J_{Ix}) \\ & \cdot(\dot{\omega}_{Bx}c_\eta - \dot{\omega}_{By}s_\eta + \omega_{Oy}\omega_{Ox}\tan\varepsilon + \omega_{Oy}\omega_{Bz}) \\ & + K_{Of}(s_\varepsilon\omega_{Ox} + c_\varepsilon\omega_{Bz}) \\ & - \left[\frac{1}{c_\varepsilon}\left(J_{Oz}+s_\varepsilon^2 J_{Ix}\right) + c_\varepsilon(J_{Oy}-J_{Ox})\right]\omega_{Ox}\omega_{Oy} \\ & + c_\varepsilon K_{O\omega}\int_0^t(\omega_{Ox}(\tau)\tan\varepsilon(\tau) + \omega_{Bz}(\tau))\,d\tau \end{aligned} \tag{A2}$$

$$g_y(t) = c_\varepsilon(J_{Iy}-J_{Ix}) - \frac{1}{c_\varepsilon}\left(J_{Oz}+s_\varepsilon^2 J_{Ix}\right) \tag{A3}$$

and

$$g_{yz}(t) = (J_{Oz}+J_{Ix})\tan\varepsilon - c_\varepsilon s_\varepsilon(J_{Iz}-J_{Ix}). \tag{A4}$$

APPENDIX B

This derivation follows that presented using the Gronwell–Bellman Lemma [7, Th. 16]. The vector norm inequality was given by (35), or

$$\ell(t) \le \beta K_O e^{-\lambda t} + \int_0^t \beta e^{-\lambda(t-\tau)}((K_J|\omega_{Ox}|_{\max} + K_F)\ell(\tau))\,d\tau. \tag{B1}$$

Multiplying by $e^{\lambda t}$ and dividing by β, one obtains

$$\left(\frac{1}{\beta}\right) e^{\lambda t}\ell(t) \le K_O + \int_0^t e^{\lambda\tau}((K_J|\omega_{Ox}|_{\max} + K_F)\ell(\tau))\,d\tau. \tag{B2}$$

Dividing the left side of this expression by the right side and multiplying by $\beta(K_J|\omega_{Ox}|_{\max} + K_F)$ results in

$$\frac{(K_J|\omega_{Ox}|_{\max} + K_F)e^{\lambda t}\ell(t)}{K_O + \int_0^t e^{\lambda\tau}((K_J|\omega_{Ox}|_{\max} + K_F)\ell(\tau))\,d\tau} \le \beta(K_J|\omega_{Ox}|_{\max} + K_F).$$

The left hand side can be expressed as the derivative of the natural log of the quantity in the denominator, or

$$\frac{d}{dt}\left\{\mathrm{Ln}\left(K_O + \int_0^t e^{\lambda\tau}((K_J|\omega_{Ox}|_{\max} + K_F)\ell(\tau))\,d\tau\right)\right\} \le \beta(K_J|\omega_{Ox}|_{\max} + K_F).$$

Integrating and raising each side to the power e results in

$$K_O + \int_0^t e^{\lambda\tau}((K_J|\omega_{Ox}|_{\max} + K_F)\ell(\tau) + K_O D_{\max})\,d\tau \le K_O e^{\int_0^t(\beta(K_J|\omega_{Ox}|_{\max}+K_F))\,d\tau}.$$

From (B2), one then has

$$\left(\frac{1}{\beta}\right) e^{\lambda t}\ell(t) \le K_O e^{[\beta(K_J|\omega_{Ox}|_{\max}+K_F)t]}$$

or

$$\ell(t) \le \beta K_O e^{(-\lambda-\beta(K_J|\omega_{Ox}|_{\max}+K_F))t}.$$

ACKNOWLEDGMENT

The authors would like to thank the reviewers whose critical analysis and suggestions brought insight into the final editing of this paper.

REFERENCES

[1] A. K. Rue, "Stabilization of precision electro-optical pointing and tracking systems," *IEEE Trans. Aerosp. Electron. Syst.*, vol. AES-5, pp. 805–819, Sept. 1969.

[2] ——, "Precision stabilization systems," *IEEE Trans. Aerosp. Electron. Syst.*, vol. AES-10, pp. 34–42, Jan. 1974.

[3] B. Friedland and D. Haessig, Jr., "On modeling and simulation of friction," *ASME J. Dyn. Syst., Meas., Contr.*, vol. 113, pp. 354–362, 1991.

[4] W. J. Bigley and F. Schupan, "Wide-band base motion isolation control for a mobile platform," in *Proc. 1987 American Control Conference*, Minneapolis, MN, June 10, 1987.

[5] C. D. Walrath, "Adaptive bearing friction compensation based on recent knowledge of dynamic friction," *Automatica*, vol. 20, pp. 717–727, 1984.

[6] B. Li, D. Hullender, and M. DeRenzo, "Nonlinear induced disturbance rejection in inertial stabilization systems," *IEEE Trans. Contr. Syst. Technol.*, vol. 6, pp. 421–427, May 1998.

[7] N. Balabanian and T. Bickart, *Electrical Network Theory*. New York: Wiley, 1969, pp. 727–767.

Peter J. Kennedy (M'76) received the B.S. degree in mechanical engineering from Lafayette College, Easton, PA, in 1971, the M.S. degree in industrial engineering from Lehigh University, Bethlehem, PA, in 1973, and the M.S. degree in electrical engineering from Fairleigh Dickenson University, Teaneck, NJ, in 1978.

He has worked in the area of pointing, tracking, and stabilization for the U.S. Army Electronic Warfare Laboratory, Bell Laboratories, SciTec, Inc., Northrop Grumman Corporation, and is presently employed with David H. Pollock Consultants, Inc., Westwood, NJ.

Mr. Kennedy is a licensed professional engineer and a member of the National Society of Professional Engineers, and the Instrumentation, Systems, and Automation Society (ISA).

Rhonda L. Kennedy (M'02) received the B.S. degree in mathematics from Phillips University, Enid, OK, in 1979 and the M.S. degree in operations research from Texas Tech University, Lubbock, TX, in 1981.

She was with Bell Laboratories from 1981 to 1983. Currently she is working in the area of statistical analysis, modeling and interface design for simulation of EO/IR sensor systems, and real-time simulations of end-to-end countermeasure systems. She is presently employed with David H. Pollock Consultants, Inc., Westwood, NJ.